Supporting Information:

Solid-state Synthesis of Single-phase Nickel Monophosphosulfide for Oxygen Evolution Reaction

Miao Wang[ab], Ali Saad[ab], Xiaoguang Li[a], Tao Peng[ab], Qi-Tao Zhang[c], Mohan Kumar[ab], Wei Zhao[a] *

[a] Institute for Advanced Study, Shenzhen University, Shenzhen 518060, China

[b] College of Physics and Optoelectronic Engineering, Shenzhen University, Shenzhen 518060, China

[c] International Collaborative Laboratory of 2D Materials for Optoelectronics Science and Technology of Ministry of Education, Institute of Microscale Optoelectronics, Shenzhen University, Shenzhen 518060, China

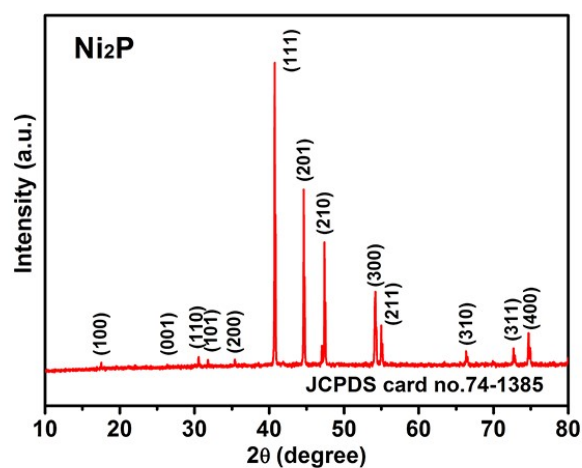**Figure S1** Schematic of quartz ampoule with the well-mixed reactants inside.

Figure S2 Powder X-ray diffraction pattern of the Ni$_2$P. The diffraction peaks can be indexed well by hexagonal Ni$_2$P (JCPDS card no. 74-1385). No obvious impurity phase can be observed in the pattern.
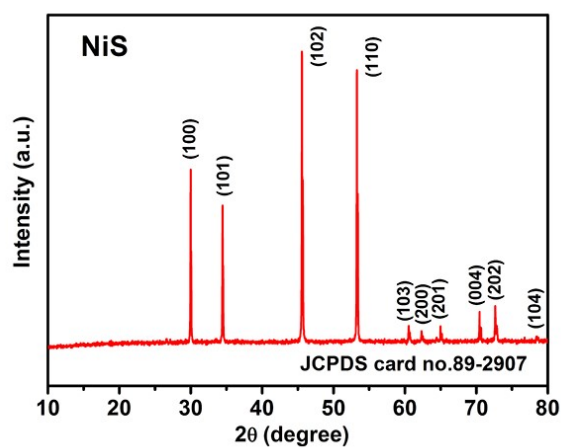

Figure S3 Powder X-ray diffraction pattern of the NiS. The diffraction peaks can be indexed well by hexagonal NiS (JCPDS card no. 89-2907). No obvious impurity phase can be observed in the pattern.
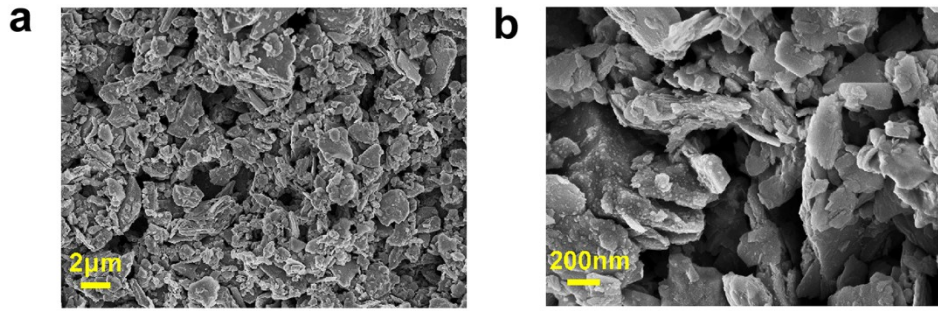
Figure S4 (a) low-magnified, and (b) high-magnified SEM images of the as-synthesized NiPS sample. It is found that the NiPS sample shows an uneven plate-like morphology.
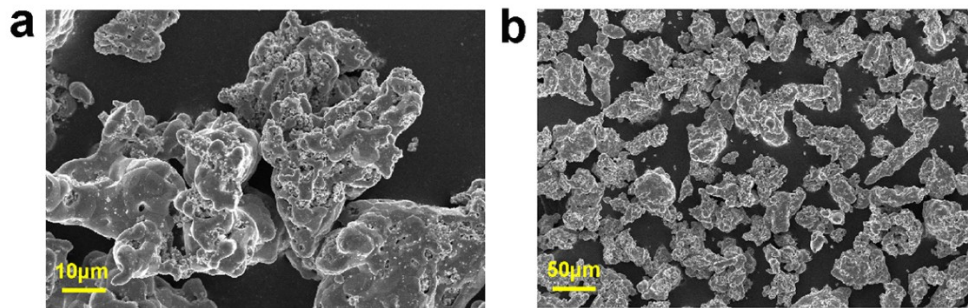

Figure S5 (a) low-magnified, and (b) high-magnified SEM images of the as-synthesized Ni_2P sample.
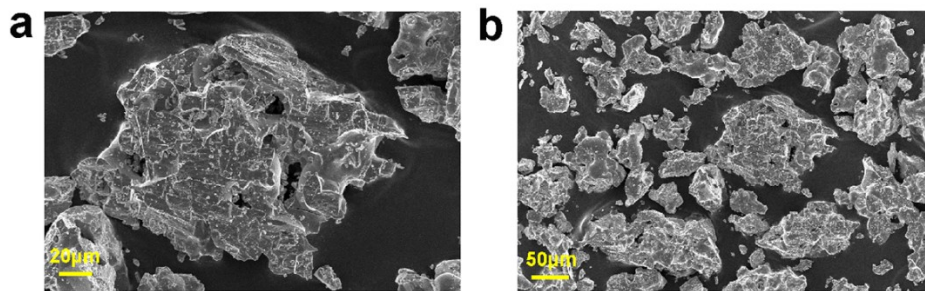

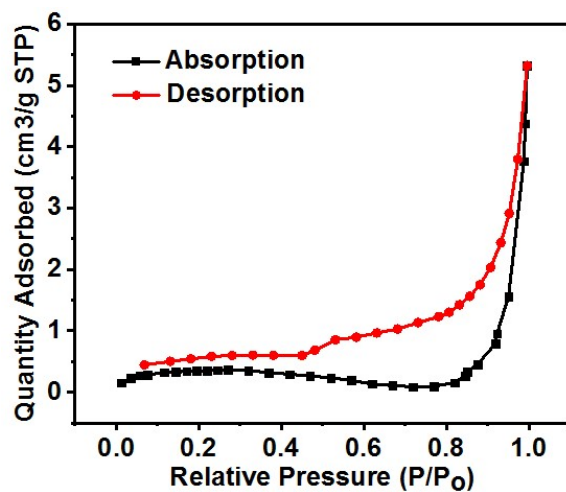**Figure S6** (a) low-magnified, and (b) high-magnified SEM images of the as-synthesized NiS sample.

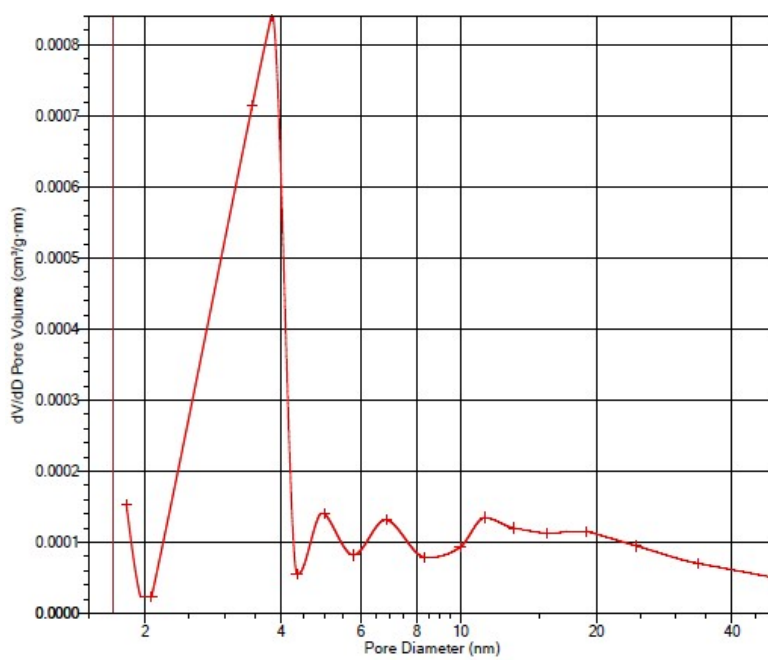**Figure S7** Nitrogen adsorption-desorption isotherms for as-synthesized NiPS sample.

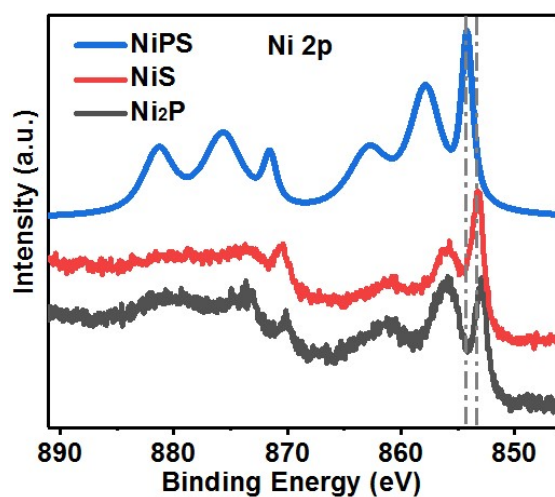**Figure S8** Pore size distribution plot for as-synthesized NiPS sample.

Figure S9 X-Ray photoelectron spectral regions for Ni 2p levels of the as-synthesized NiPS, Ni_2P and NiS samples.

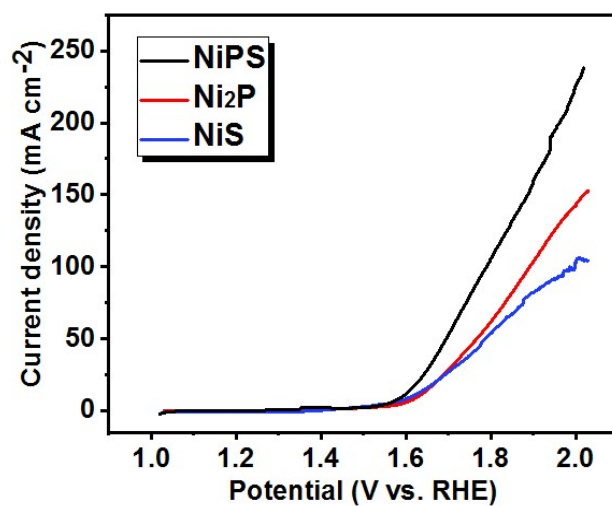**Figure S10** LSV plots of the NiPS, Ni_2P and NiS for OER in 1.0 M KOH solution.
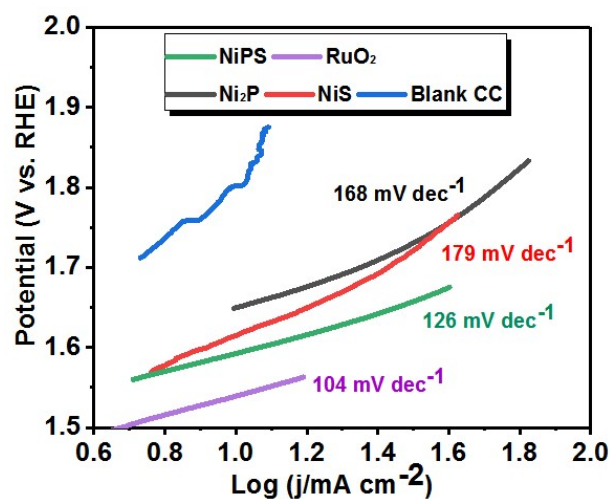
Figure S11 Tafel plots of the NiPS, commercial RuO_2, Ni_2P, NiS and blank carbon cloth for OER in 1.0 M KOH solution.
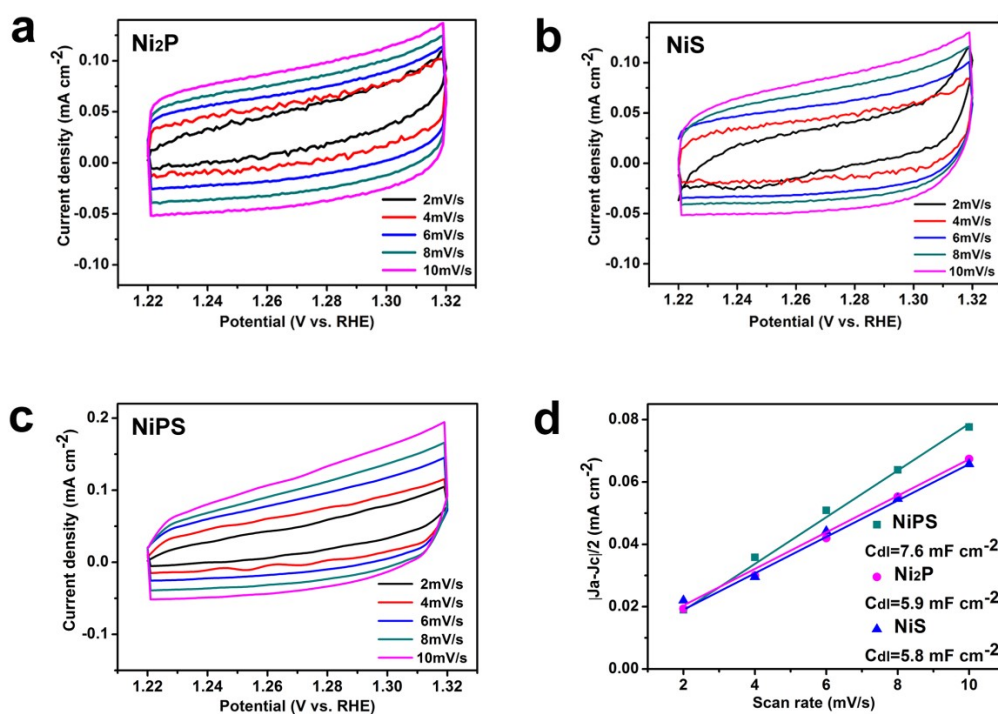

Figure S12 (a-c) CV curves of Ni_2P, NiS and NiPS at different scan rates. (d) The double-layer capacitances of NiPS, Ni_2P and NiS.

The ECSA can be calculated from the C_{dl} according to the ratio:

$$ESCA = \frac{C_{dl}}{C_S}$$

Where Cs is the specific capacitance, chosen as Cs = 0.040 mF·cm^{-2} in 1 M KOH based on reported values.[1-4]
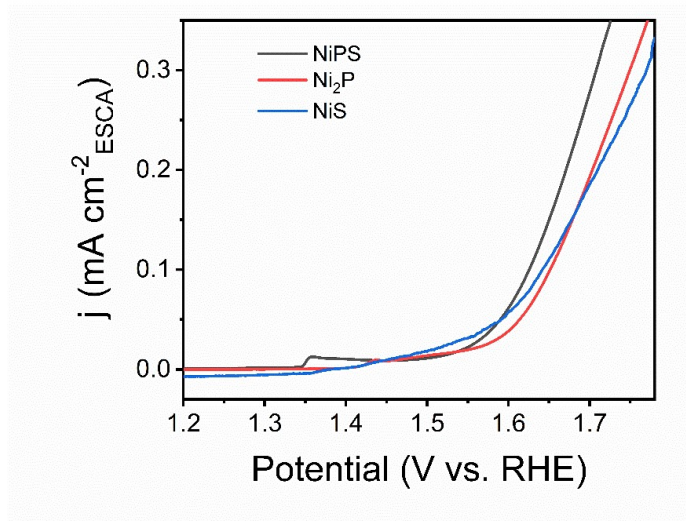

Figure S13 The electrochemically active surface area (ECSA) for linear-sweep voltammetry (LSV) for NiPS, Ni$_2$P and NiS

Table S1 Parametres (C$_{dl}$, ESCA and intrinsic activity) for each catalyst investigated in 1 M KOH.

Catalyst	NiPS	Ni$_2$P	NiS
C$_{dl}$ (mF cm^{-2})	7.6	5.9	5.8
ESCA (cm^2)	190	147.5	145
Intrinsic catalyst activity (mA cm^{-2}) η= 430mV	0.1074	0.082	0.065

References:

1. Zhang, Y.; L, Gao.; Hensen, E.J.M.; Hofmann, J.P., Evaluating the Stability of Co$_2$P Electrocatalysts in the Hydrogen Evolution Reaction for Both Acidic and Alkaline Electrolytes. *ACS Energy Lett*. **2018**, 3, 1360−1365.

2. Wang, H.; Zhang, X.; Xie, Y., Photocatalysis in two-dimensional black phosphorus: the roles of many-body effects. *Acs Nano* **2018**, *12(10)*, pp.9648-9653.

3. Liu, M.; Kong, L.J.; Wang, X.M.; He, J.; Bu, X.H., "Engineering bimetal synergistic electrocatalysts based on metal–organic frameworks for efficient oxygen evolution." *Small* **2019**, *15*, no. 45: 1903410.

4. Zeng, L.Y.;, Sun, K.A.; Wang, X.B.; Liu, Y.Q.; Pan, Y.; Liu, Z.; Cao, D.W.; Song, Y.; Liu, S.H.; Liu. C.G.,"Three-dimensional-networked Ni_2P/Ni_3S_2 heteronanoflake arrays for highly enhanced electrochemical overall-water-splitting activity." *Nano Energy* **2018**, *51*, 26-36.
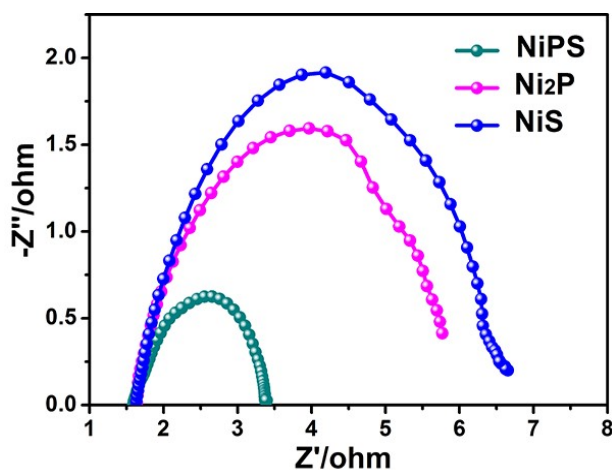
Figure S14 EIS curves of NiPS, Ni_2P and NiS.
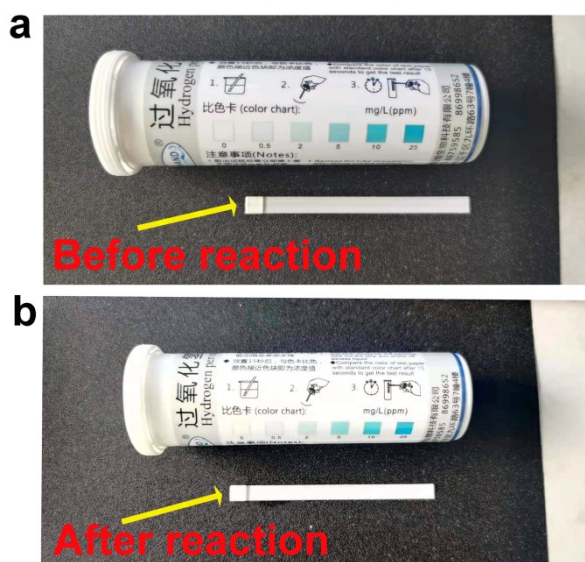
Figure S15 Results of hydrogen peroxide (H_2O_2) rapid test card of the as-synthesized catalysts obtained in this work before and after OER.

Figure S16 (a-c) Low-magnified and high-magnified SEM images of the NiPS after OER.

Figure S17 XPS spectra of Ni 2p spectrum of the NiPS after OER, indicating the main formation of higher valence Ni-based intermediate.
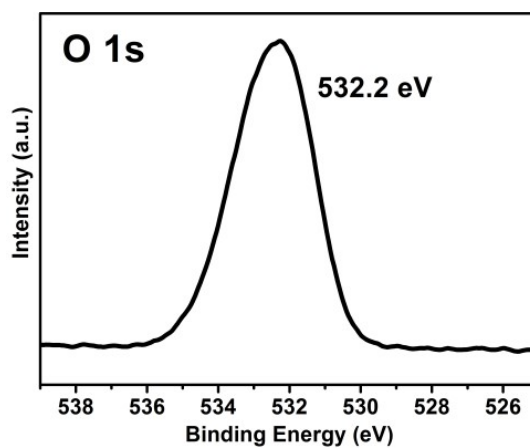
Figure S18 XPS spectra of O 1s spectrum of the as-prepared NiPS sample.

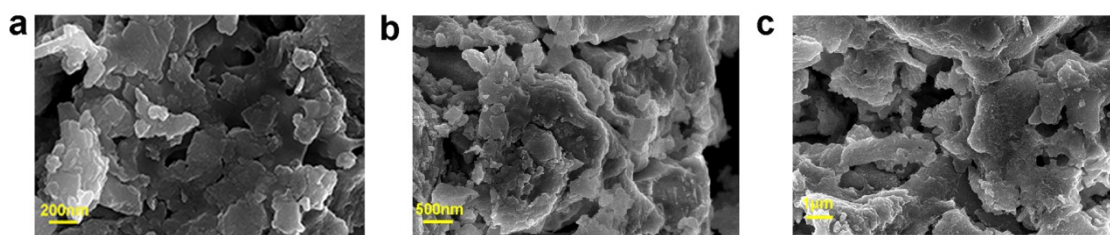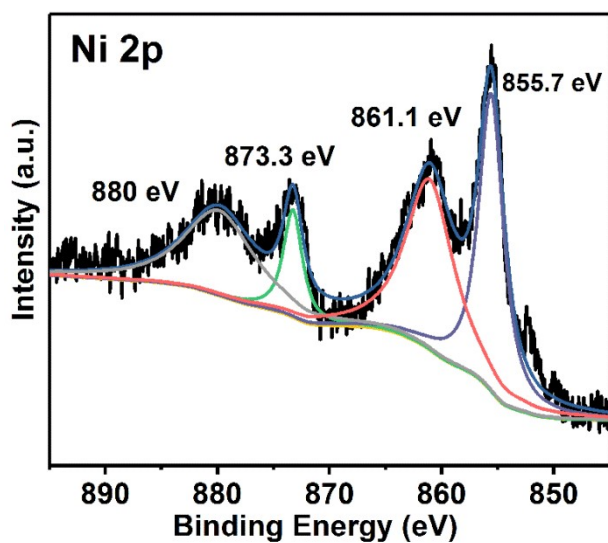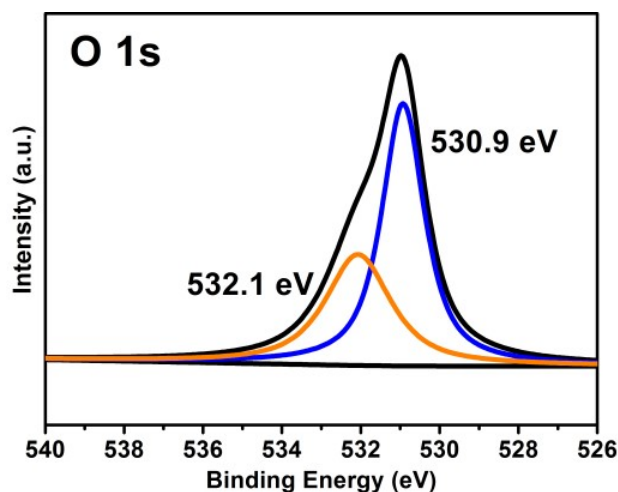**Figure S19** XPS spectra of O 1s spectrum of the NiPS after OER. And the peak observed at ~ 530.9 eV demonstrating the generation of hydroxyl-based functional groups during the OER process.
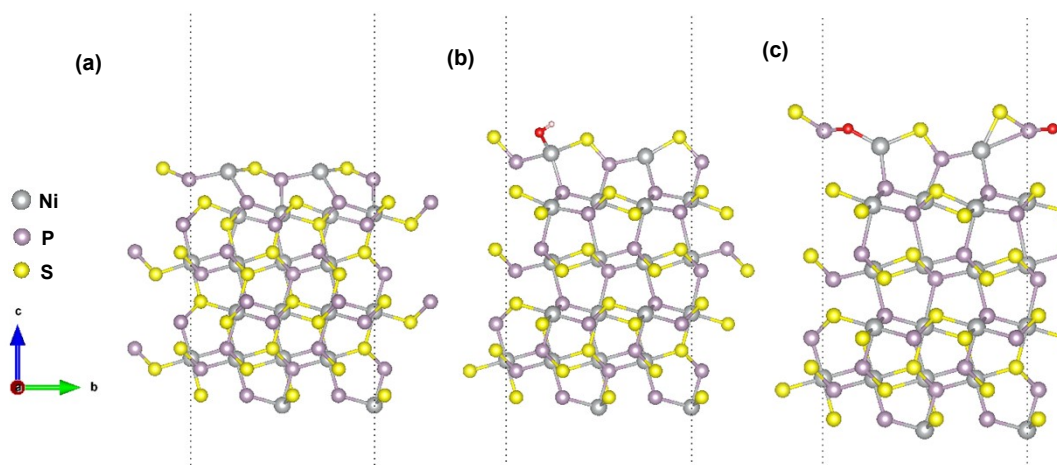
Figure S20 The structures of vacant site, OH* and O* at the (200) surface of NiPS model.

The molecular orbital interaction between Ni and O was schematically drawn in **Figure S21**, from which we can see that the π-type interactions between Ni and O are strongly repulsive because interactions between π-type orbitals of Ni (d_{xz}, d_{yz}) and O (p_x,p_y) lead to formation of two occupied π bonding orbitals and another two occupied $\pi*$ anti-bonding orbitals which are energetically unfavorable due to two-center four-electrons interactions. In other words, Ni can't form double bond with O.
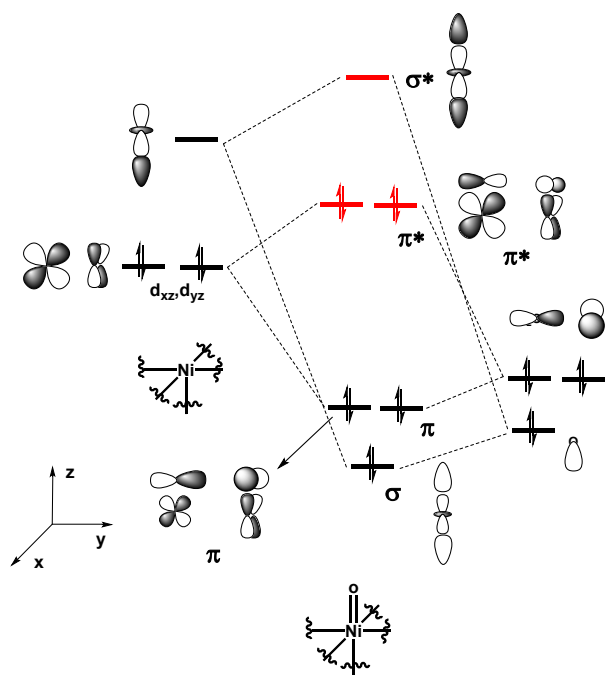
Figure S21 Orbital interaction analysis of Ni-O bond in NiPS model.
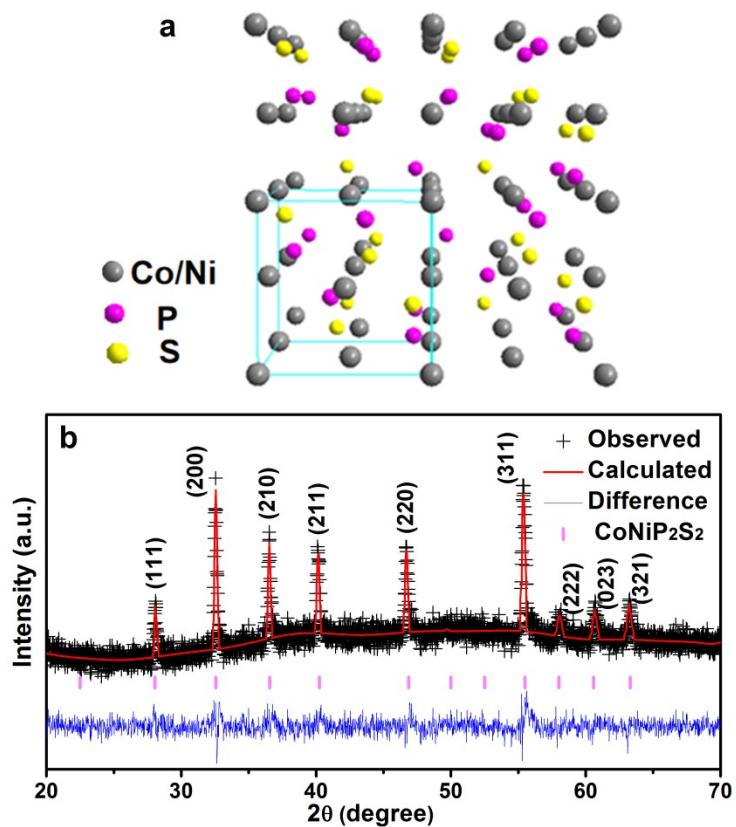
Figure S22 (a) The schematic view of the crystal structure of the $CoNiP_2S_2$. (b) Measured (crosses) and calculated (red solid line) XRD patterns for $CoNiP_2S_2$. Bragg peak positions are indicated by short vertical bars.

The bottom of the figure shows the differences between measured and calculated intensities.

Table S2 Crystallographic Parameters from the Powder XRD Refinement of $CoNiP_2S_2$ sample at 300K.

| atom	site	x	y	z	occup.	U_{iso} (fixed)
Co	4a	0	0	0	0.50	e^{-5}
Ni	4a	0	0	0	0.50	e^{-5}
P	4a	0.61	0.61	0.61	1.00	$2 \times e^{-5}$
S	4a	0.39	0.39	0.39	1.00	$2 \times e^{-5}$

Space group: $P2_13$; a=b=c=5.5118Å, V=167.4481Å^3, R_{wp}=0.0441, R_p=0.0343, χ^2=1.277.

The morphology of the as-synthesized $CoNiP_2S_2$ sample was observed using SEM, and **Figure S23**(a,b) display the representative SEM images with different magnification. It is found that the microstructure of the $CoNiP_2S_2$ sample shows a lumpy aggregation without regular morphology. To further identify the microstructures of the $CoNiP_2S_2$ sample, TEM images were also collected, as shown in **Figure S23**(c,d). The elemental distribution of the as-synthesized $CoNiP_2S_2$ was further investigated by scanning TEM-energy dispersive X-ray (STEM-EDX) and the results are shown in **Figure S23**(e-i). These images show that Co, Ni, P and S elements are uniformly distributed in the $CoNiP_2S_2$ sample.
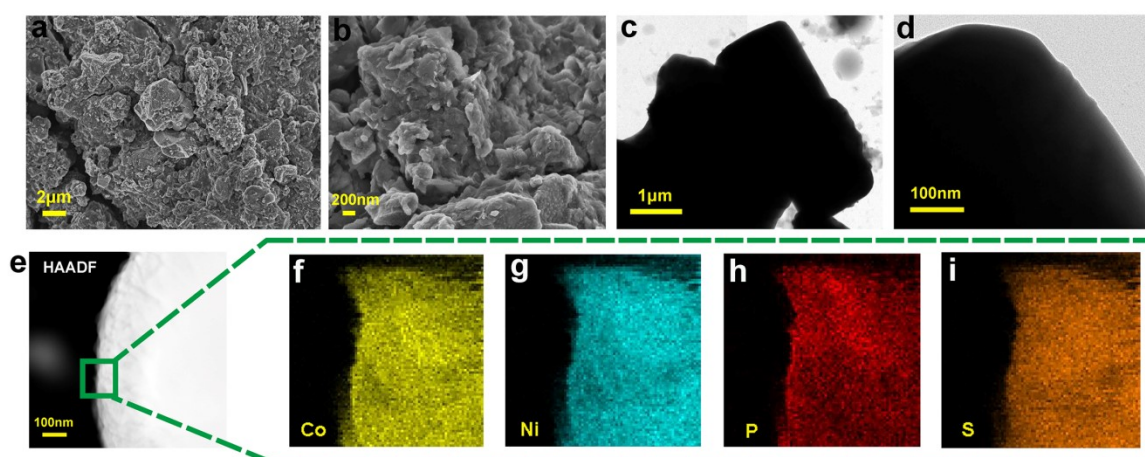

Figure S23 (a) Low-magnified and (b) high-magnified SEM images of the $CoNiP_2S_2$ sample with different magnification. (c) low-magnified and (d) high-magnified TEM images of the $CoNiP_2S_2$ sample. (e-i) HAADF-STEM and corresponding EDX mapping images of the $CoNiP_2S_2$ sample.

X-ray photoelectron spectroscopy (XPS) was also performed to further analyze the bonding characteristics as well as the composition of as-synthesized sample. As shown in **Figure S24**a, the Co 2p core level peaks can be divided into two satellite peaks and spin-orbit doublets. The peaks at around 778.7 eV and 793.7 eV are attributed to the $2p_{3/2}$ and $2p_{1/2}$ of Co^{3+}, respectively. The peaks situated at 781.2 eV and 782.7 eV can be ascribed to $2p_{3/2}$ of Co^{2+}, and the peaks at 797.7 eV and 799.8 eV can be ascribed to $2p_{1/2}$ of Co^{2+}, respectively, while the other two peaks at 786.6 eV and 803.9 eV are satellites.[1-3] **Figure S24**b indicates that the Ni 2p spectrum can be well-fitted with three spin-orbit doublets accompanied with two obvious shakeup satellites (862.8 eV and 881.1 eV), identified as Ni $2p_{1/2}$ and Ni $2p_{3/2}$ signals. Deconvolution of the Ni $2p_{3/2}$ peak corresponds to three energy bands: 853.8 eV for Ni^{2+} and (856.8 eV and 858.7 eV) for Ni^{3+}, meanwhile the Ni $2p_{1/2}$ peak exists in other three energy bands: 871 eV for Ni^{2+} and (874.4 eV and 876.6 eV) for Ni^{3+}.[1,4,5]
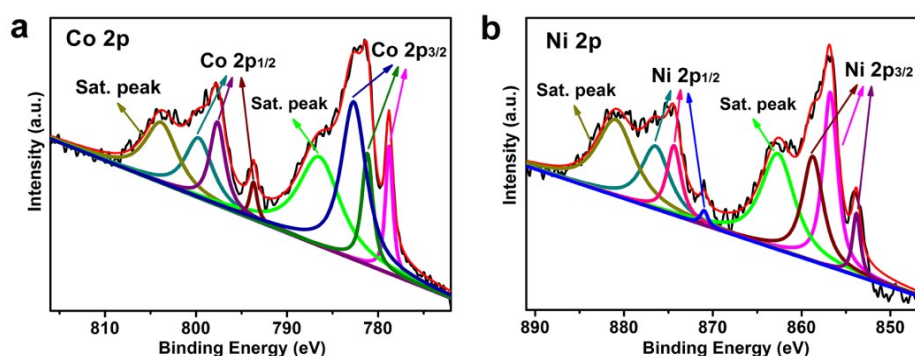
Figure S24 X-Ray photoelectron spectral regions for (a) Co 2p and (b) Ni 2p levels of the as-synthesized $CoNiP_2S_2$ sample.

The P 2p core level of XPS spectrum (**Figure S25**) has its spin-orbit doublet in the $2p_{3/2}$ and $2p_{1/2}$ peaks positioned at 129.4 eV and 130.1 eV.[6] In addition, **Figure S26** displays the S 2p spectrum, where S ($2p_{3/2}$) and S ($2p_{1/2}$) are located at 162.5 eV and 163.7 eV, respectively.[7]
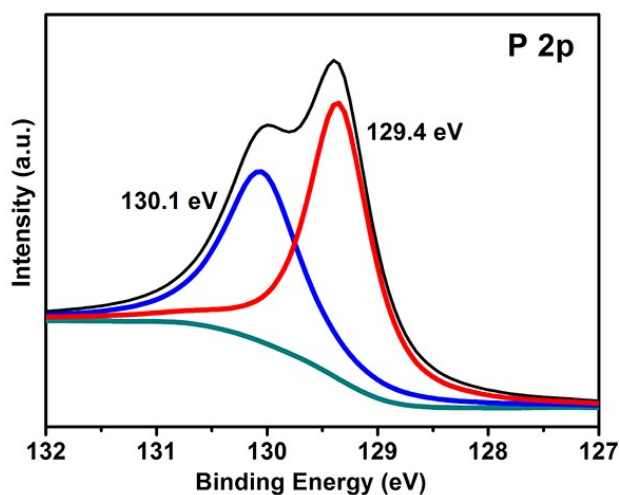
Figure S25 X-Ray photoelectron spectral region for P 2p level of the CoNiP$_2$S$_2$ sample.
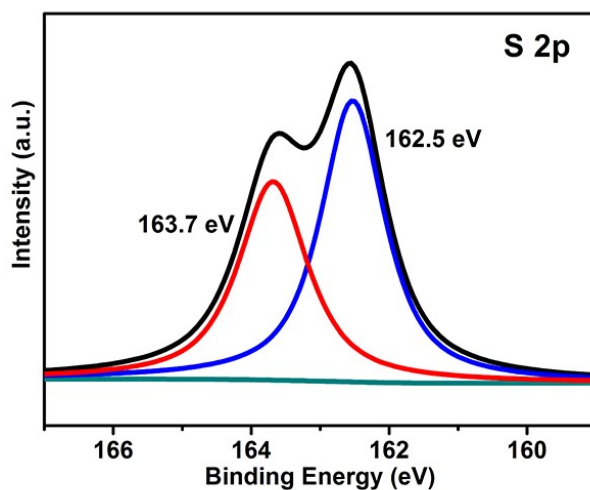

Figure S26 X-Ray photoelectron spectral region for S 2p level of the CoNiP$_2$S$_2$ sample.

References:

1.   Zhao, M.; Zhu, L.; Fu, B.; Jiang, S.; Zhou, Y.; Song, Y., Sodium ion storage performance of NiCo$_2$S$_4$ hexagonal nanosheets. *Acta Phys. -Chim. Sin.* **2019,** *35* (2), 193-199.

2.   Pan, Y.; Sun, K.; Liu, S.; Cao, X.; Wu, K.; Cheong, W.-C.; Chen, Z.; Wang, Y.; Li, Y.; Liu, Y.; Wang, D.; Peng, Q.; Chen, C.; Li, Y., Core-shell ZIF-8@ZIF-67-Derived CoP nanoparticle-embedded N-doped carbon nanotube hollow polyhedron for efficient overall water splitting. *J. Am. Chem. Soc.* **2018,** *140* (7), 2610-2618.

3.   Liu, P.; Lin, Y.; Li, J.; Wang, Z.; Nauman Ali, R.; Song, L.; Xiang, B.; Lu, Y., Engineering ternary pyrite-type CoPS nanosheets with an ultrathin porous structure for efficient electrocatalytic water splitting. *ChemElectroChem* **2019,** *6* (11), 2852-2859.

4.   Zhang, J.; Cui, R.; Li, X. a.; Liu, X.; Huang, W., A nanohybrid consisting of NiPS$_3$ nanoparticles coupled with defective graphene as a pH-universal electrocatalyst for efficient hydrogen evolution. *J. Mater. Chem. A* **2017,** *5* (45), 23536-23542.

5.   Li, X.; Xin, M.; Guo, S.; Cai, T.; Du, D.; Xing, W.; Zhao, L.; Guo, W.; Xue, Q.; Yan, Z., Insight of synergistic effect of different active metal ions in layered double hydroxides on their electrochemical behaviors. *Electrochim. Acta* **2017,** *253*, 302-310.

6.   Peng, B.; Xu, Y.; Liu, K.; Wang, X.; Mulder, F. M., High-performance and low-cost sodium-ion anode based on a facile black phosphorus-carbon nanocomposite. *ChemElectroChem* **2017,** *4* (9), 2140-2144.

7.   Kim, Y.; Hwang, H.; Lawler, K.; Martin, S. W.; Cho, J., Electrochemical behavior of Ge and GeX$_2$ (X = O, S) glasses: Improved reversibility of the reaction of Li with Ge in a sulfide medium. *Electrochim. Acta* **2008,** *53* (15), 5058-5064.

The electrocatalytic performance of CoNiP$_2$S$_2$ catalyst for OER was studied in alkaline medium (1.0 M KOH). The iR-corrected LSV curves of OER (**Figure S27**a) reveal that the CoNiP$_2$S$_2$ only needs 376 mV overpotential to generate a current density of 20 mA cm^{-2}. Based on the LSV curves, the Tafel plots are also built (**Figure S27**b). The CoNiP$_2$S$_2$ catalyst shows a Tafel slope of 143 mV dec^{-1}, implying a good reaction kinetics for the CoNiP$_2$S$_2$ catalyst in an oxygen evolution process, although higher in comparison with that in the commercial RuO$_2$ (98 mV dec^{-1}). Stability is another important characteristic for evaluation of catalyst performance. Hence, continuous CV measurements of CoNiP$_2$S$_2$ were carried out for 5000 cycles in 1.0 M KOH solution at scan rate of 50 mV s^{-1}. The polarization curves obtained before and after cycling (**Figure S27**c) revealed that no obvious activity degradation was observed. The charge transfer resistance (Rct) is related to the semicircle observed in the Nyquist curve, as shown in **Figure S27**d. It is found that the obviously smaller semicircle is obtained for CoNiP$_2$S$_2$, suggesting the smaller value of Rct, and thus the better OER kinetics among the tested catalysts.
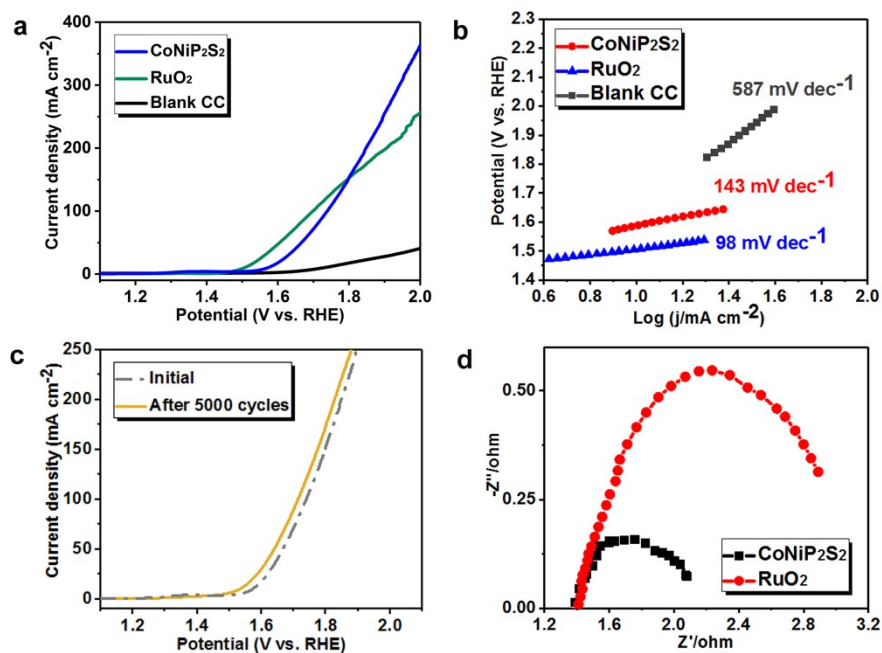

Figure S27 (a) LSV curves of the CoNiP$_2$S$_2$, commercial RuO$_2$ and blank carbon cloth in 1.0 M KOH solution (scan rate 5 mV s^{-1}) for the OER. (b) Tafel plots of the CoNiP$_2$S$_2$, commercial RuO$_2$, and blank carbon cloth for OER in 1.0 M KOH solution. (c) Polarization curves of the CoNiP$_2$S$_2$ before and after 5000 CV cycles. (d) Electrochemical impedance spectra (EIS) Nyquist plots of the CoNiP$_2$S$_2$ and commercial RuO$_2$.

Figure S28 and Figure S29 display the microstructural characterizations (SEM, TEM and EDX-mapping) of the CoNiP$_2$S$_2$ catalyst after OER, showing a similar irregular morphology.
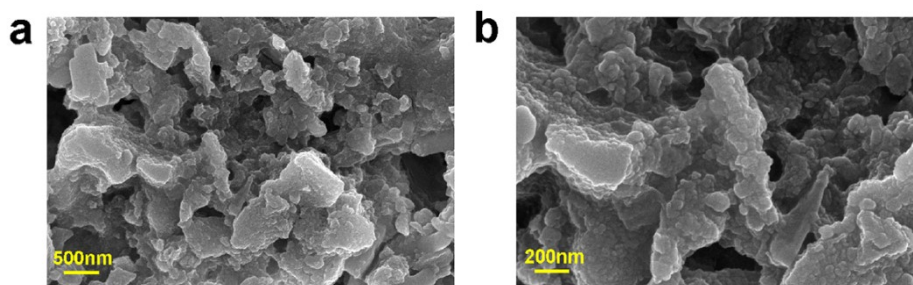

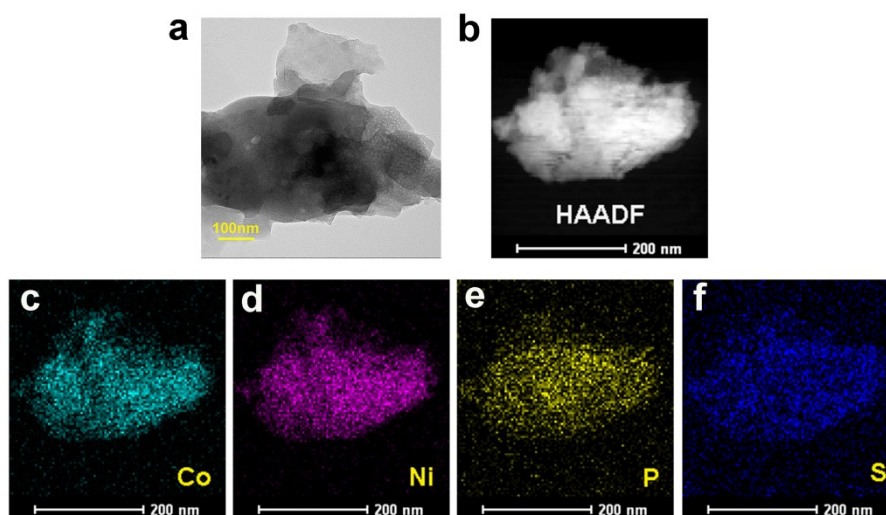**Figure S28** (a-b) Low-magnified and high-magnified SEM images of the CoNiP$_2$S$_2$ after OER.

Figure S29 (a) TEM image of the CoNiP$_2$S$_2$ after OER. (b-f) HAADF-STEM and corresponding EDX-mapping images of the CoNiP$_2$S$_2$ after OER.